Phenomenology of a two-phase laminar flame interacting with a heated cylinder

Olivier Thomine, Guodong Gai, Abdellah Hadjadj, Sergey Kudriakov

Version of Record: https://www.sciencedirect.com/science/article/pii/S0017931020337996
Manuscript_1190a0e98d5842e8cbcf7a71eefdbb4a

Phenomenology of a two-phase laminar flame interacting with a heated cylinder

Olivier Thomine[c], Guodong Gai[a,b,*], Abdellah Hadjadj[b], Sergey Kudriakov[a]

[a] *DEN-DM2S-STMF, Commissariat à l'Énergie Atomique et aux Énergies Alternatives, Université Paris-Saclay, 91191 Gif-sur-Yvette, France*
[b] *University of Normandy, INSA, CORIA UMR - 6614 CNRS, 76000 Rouen, France*
[c] *Aix Marseille Univ, Université de Toulon, CNRS, LIS (UMR 7020), Avenue Escadrille Normandie-Niemen, F-13397 Marseille Cedex 20, France*

Abstract

In this work, the interaction between a two-phase laminar flame and a heated cylinder is investigated numerically. Different physical phenomena are considered, such as droplets/cylinder collision, droplets evaporation, flame ignition and stabilization. Several important parameters appearing in the interaction are discussed. The Stokes number is proved to be of significant importance on the droplet segregation. The region of highest density of liquid fuel in the vicinity of the cylinder is analyzed as to study the droplet segregation in the two-phase flow. As a result of evaporation, the droplet segregation can effectively change the gas mixtures near the cylinder. The spray droplets with small Stokes numbers show weak evaporation capacity on the cylinder surface. It is found that the fuel gas density increases with higher Stokes number and a flame detachment is noticed.

Keywords: Spray droplets, Laminar flame, Stokes number, Submerged cylinder

1. Introduction

The interaction between spray droplets and heated solid walls is an interesting subject of research that has several industrial applications, such as fuel preparation processes [1], flame ignition [2] and stabilization [3], and spray cooling [4]. This topic has been an active research field for decades [5–9]. The ignition of flammable liquide by hot surfaces is widely applied in automotive and aviation industries. Thin filaments are also used to stabilize the flame in many combustion studies [10, 11]. The presence of a heat source in the fuel-air mixture enables the ignition and the stabilization of a flame. This methodology is also widely used in experimental studies of stationary flames [12, 13].

Earlier studies regarding the effects of submerged bodies on particle clouds were carried out by Landahl and Herrmann [1]. The objective was to determine the important physical parameters involved in the collisions between particles and submerged bodies. The case of a cylinder embedded in an air flow charged with liquid droplets was investigated by Pawlowski *et al.* [14], considering several interaction parameters such as particle sizes, flow velocity, etc. A computational method

*Corresponding author
Email address: guodong.gai@insa-rouen.fr (Guodong Gai)

was proposed to quantify the droplets settling on the cylinder surface. Karl *et al.* [5] summarized different dynamic droplets/heated-wall interaction processes and highlighted the effects of the impinging energy and the angle of spray droplets.

One of the important cases of spray/submerged-body interaction is the study of droplets impingement on heated surfaces. The heat transfer between the droplets and the submerged body has been much investigated [15, 16], and it turns out that the presence of droplets in the boundary layer surrounding the immersed body has a significant impact on heat exchanges between the cylinder and the spray droplets [17–19].

During the combustion processes, diverse studies have focused on the behavior of a stabilized single-phase flame in the wake of a submerged body [20, 21]. Various experiments were performed to analyze the ignition and the extinction limit of gaseous flames interacting with submerged bodies [2, 22]. For instance, Stathopoulos *et al.* [11] studied the ignition of ethanol-oxygen mixtures using a hot-wire anemometry technique. The importance of the bulk temperature, fuel composition and droplet loading were discussed. Yuan *et al.* [23] investigated experimentally the ignition of hydraulic sprays by heated surfaces. The cloud properties such as droplet size, surface temperature, degree of atomization were proved to be important for the interaction. Additional studies were carried out in order to analyze the flame stabilization in the wake region behind a cylinder [24]. Recently, the combustion of gaseous or liquid fuel in micro- or meso-scale tubes with wire mesh has been intensively investigated [25, 26]. An important component in a micro-power generator is the micro-combustor where a wire mesh can be used in order to enhance the flame-wall thermal interaction. It is difficult to keep a stable flame inside a micro-combustor as a result of high heat loss rate and small residence time. The interaction between the fuel droplets and the wire mesh can be interesting in terms of the flame stabilization.

However, numerical investigations on submerged bodies interacting with sprays and flames are scarcely available in the literature. Some phenomena were investigated, such as droplets evaporation, collisions and heat transfer between droplets and submerged body, but the main physical mechanisms are still not fully understood.

In this study, we propose to investigate numerically these flows in order to shed more light into these complex phenomena and to assess the topology of two-phase flames in the wake of a heated cylinder submerged in a fuel droplet-laden flow. This is a simple but representative configuration for the investigation of the interaction between the fuel droplets and a heated submerged body. Using this configuration, we want to identify the key parameters for the interaction processus and try to evaluate their effects on the flame structure. The Stokes number is considered to be very important for the interaction processes in this problem. The analytical study of Greenberg *et al.* shows that the droplets with higher Stokes number can contribute to the increase of the flame area leading to a higher burning velocity [27]. Experiments show that the inertia of the fuel droplets of higher Stokes number can increase the burning rate and this enhancement can be more significant with increasing turbulence [28]. Numerical simulations also show that a higher Stokes number can increase the local fuel concentration inside a spherical expanding flame, leading to a higher burning rate, and strengthened by turbulence [29]. Several other parameters are also involved, such as the temperature of the cylinder, the Reynolds number of the gas, the diameter and the density of the droplets.

This paper is organized as follows. Section 2 discusses the mathematical equations and the physical models used in the simulations, while Section 3 presents the main configuration along with the boundary and the initial conditions. Section 4 examines the effects of Stokes number on

the segregation of the droplets. The evolution of the gas mixtures along with a comprehensive analysis of the flame topology during the combustion process is briefly discussed in Section 5. Finally, the main conclusions are drawn in Section 6.

2. Governing equations and numerical modeling

2.1. Governing equation

The governing equations for the gaseous phase are the Navier-Stokes equations under the Low Mach Number (LMN) approximation, consisting of multi-species, momentum and energy transport equations. The gas follows the ideal gas law.

The conservation of mass in a multi-species flow can be established by considering the transport of different species k of the mass fraction Y_k with $\sum Y_k = 1$. The transport equation of the species k is given by:

$$\frac{\partial \rho Y_k}{\partial t} + \frac{\partial \rho u_i Y_k}{\partial x_i} = \frac{\partial}{\partial x_i}\left(\rho D_k \frac{\partial Y_k}{\partial x_i}\right) + \dot{\omega}_k \,, \tag{1}$$

where D_k is the diffusivity of the species k, $\dot{\omega}_k$ is a combustion or evaporation source term of the species k.

The momentum transport equation is written as:

$$\frac{\partial \rho u_i}{\partial t} + \frac{\partial \rho u_i u_j}{\partial x_j} = -\frac{\partial p}{\partial x_i} + \frac{\partial \tau_{ij}}{\partial x_j}, \tag{2}$$

with ρ is the mass density of the gas, u_i the gas velocity in the direction i and τ_{ij} the viscous-stress tensor given by [30]:

$$\tau_{ij} = \mu\left[\frac{\partial u_i}{\partial x_j} + \frac{\partial u_j}{\partial x_i}\right] - \frac{2\mu}{3}\frac{\partial u_l}{\partial x_l}\delta_{ij} \,. \tag{3}$$

with μ the dynamic viscosity of the fluid.

The sensible energy e_s of the fluid is transported by the following equation:

$$\frac{\partial \rho e_s}{\partial t} + \frac{\partial \rho u_i e_s}{\partial x_i} = \frac{\partial}{\partial x_i}\left(\lambda \frac{\partial T}{\partial x_i}\right) - \frac{\partial p u_i}{\partial x_i} + \frac{\partial \tau_{ij} u_i}{\partial x_j} + \dot{\omega}_{es} \,, \tag{4}$$

where λ is the thermal conductivity of the gas flow and $\dot{\omega}_{es}$ is the source term taking into account the combustion reaction heat release. The gas-cylinder heat release and droplet evaporation are described using closure models.

2.2. Characteristics of the cloud particles

In this study, the gas phase is assumed to follow the perfect gas law. The droplets are considered as spherical with a small volume fraction that allows to neglect the collisions. The one-way formalism is applied for the momentum and heat transfer between the gas and droplets in the highly-dilute two-phase system. Only the viscous drag force is considered on the droplets, provided that the gravity is negligible compared to the drag for the droplets studied. For simplicity, the Basset force is neglected as a result of the high-density ratio of the liquid/gas phases and we assume that the particles do not spin (the Magnus force is neglected). The heat transfer due to the droplet evaporation is not considered. Whereas, the mass transfer from droplets to the gas is considered by droplet evaporation.

For a droplet with a velocity $\mathbf{V}(t)$ located at the coordinate $\mathbf{x}$ the general equation of motion reads:

$$m_p \frac{d\mathbf{V}(t)}{dt} = \sum \mathbf{F} \,, \tag{5}$$

where $m_p = \pi \rho_p d_p^3/6$ is the droplet mass and ρ_p is the droplet mass density. The Stokes drag force on the droplet can be obtained by:

$$\mathbf{F} = 3\pi \,\mu_g \, d_p \left(\mathbf{u}(\mathbf{x},t) - \mathbf{V}(t)\right) \,, \tag{6}$$

where μ_g is the dynamic viscosity of the gas. Since the diameter of the droplet is relatively small, with particle Reynolds number $Re_p = O(1)$, the drag coefficient is assumed to be the Stokes coefficient for laminar flow. The equation of motion for each droplet can be obtained:

$$\frac{d\mathbf{V}(t)}{dt} = \frac{1}{\tau_p} \left(\mathbf{u}(\mathbf{x},t) - \mathbf{V}(t)\right) \,, \tag{7}$$

where $\tau_p = \frac{\rho_p d_p^2}{18\mu_g}$ is the characteristic droplet response time.

2.3. Temperature dependent law using Artificial Temperature Indexing (AIT)

Droplet evaporation has been an active research field for decades and several evaporation models exist in the literature [31–35]. For example, the simple "d^2" law is widely used, which stipulates that the evaporation rate of the drops has no dependence on its environment. During a real evaporation process, the surface evolution of the drop is a function of the pressure, the mass fraction of the species S and the ambient temperature [36]. However, in a simplified case where the species S is relatively diluted, the pressure plays a minor role. Thus, the surface transfer parameters can be expressed solely as a function of the temperature [37, 38]. The associated transfer number $B_M(T, Y_S, p)$ can therefore be expressed independently of Y_S and p.

As a first approximation, one can consider the variation of B_M as linear with regards to the temperature T. The Artificial Temperature Indexing (AIT) model can therefore be defined by:

$$B_M(T) = \Pi \left(T(\vec{X}) - T_u\right) \,,$$

where Π is a model parameter. In the AIT model, the drop is considered to be at rest in a saturation state. The theoretical Spalding number $B_{M,0}$, for initial diameter, $d_{p,0}$ can be expressed as a function of the characteristic evaporation time τ_v:

$$B_{M,0} = \exp\left(\frac{Sc\ \rho_d d_{p,0}^2}{4Sh_c\ \mu\, \tau_v}\right) - 1 \,,$$

with $d_{p,0}$ the initial diameter of the droplets and $Sh_c = \frac{\delta_Y}{\delta_Y - d_p}$ is the convective Sherwood number where δ_Y is the diameter of the boundary layer of the species diffusion of the droplet and d_p is droplet diameter. Since the coefficient Π is based on the temperature difference between burnt (T_b) and fresh gases (T_u), one can obtain the expression:

$$\Pi = \frac{1}{T_b - T_u} B_{M,0} = \frac{1}{T_b - T_u} \left[\exp\left(\frac{Sc\ \rho_d d_{p,0}^2}{4Sh_c\ \mu\, \tau_v}\right) - 1\right] \,,$$

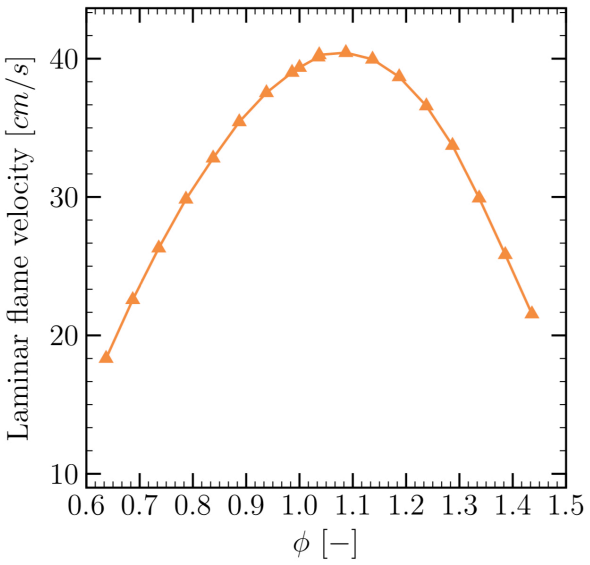

Figure 1: Laminar flame velocity for different compositions of fuel gas; comparison of experimental results: C_7H_{16}-exp (▲) and model results with K adapted to C_7H_{16} (—) [38].

Using this model, it is possible to monitor the characteristic evaporation time τ_v of the drops without interfering with their initial properties or the parameters of combustion such as equivalence ratio, reaction order, etc.:

$$\tau_v = \frac{\rho_d \, Sc \, d_{p,0}^2}{4 \, Sh_c \, \mu \, ln(1+B_M)} \, . \tag{8}$$

The evaporation of the droplets is only considered to change the gas mixture composition.

2.4. Combustion and cylinder heat release

As for the combustion model, a simple one-step reaction is used, with the reaction rate tabulated according to experimental data, for n-heptane ($n-C_7H_{16}$) droplets [38, 39]. A corrective factor K depending on equivalent ratio ϕ is introduced in Arrhenius' law so that the numerical data fit with the experimental curves which gives an expression of reaction rate in the form:

$$\dot{\omega}_R = K(\phi)\rho Y_F Y_O \frac{\Phi_s (Y_F + Y_O)^2}{(\Phi_s Y_F + Y_O)^2} \exp\left(\frac{\beta}{\alpha} - \frac{\beta}{\alpha(1-\alpha)T}\right) \, , \tag{9}$$

with $\Phi_s = \nu_O/\nu_F$, where the coefficients ν_F and ν_O are chosen such that $\nu_O + \nu_F = 1$. Y_F and Y_0 are mass fractions of the fuel and oxidant, respectively. $K(\phi)$ is a coefficient allowing to exactly match the flame speed obtained numerically to the one obtained experimentally as shown in Fig. 1. K values are chosen for different species of different equivalence ratios. The case of constant K is given for comaprison. $\alpha = (T_b - T_u)/T_b$, $\beta = \alpha T_a/T_b$, where T_a is the activation temperature, T_u and T_b are temperatures of the fresh and burnt gas, respectively.

The heat released from the cylinder is described using a mask taking valuesbetween 0 and 1 during. During one time step Δt, the energy can be calculated by the following expression:

$$\rho e_s(t+\Delta t) = M(x,y,z)\left(\rho e_s(t) + \Delta t \frac{\partial e_s}{\partial t}\right) + (1 - M(x,y,z)) e_{s,cyl}. \tag{10}$$

Parameter	Symbol	Values	Units
Air mass density	ρ_g	1.2	kg/m^3
Air viscosity	μ_g	1.81×10^{-5}	$Pa \cdot s$
Air velocity	u_0	5	m/s
Surface tension	σ_p	0.02	N/m
Droplet diameter	$d_{p,0}$	$1.8 - 12$	μm
Droplet mass density	ρ_p	679.5	kg/m^3

Table 1: Physical properties of air and n-heptane droplets.

The current numerical simulations are performed using an *in-house* compressible Navier-Stokes (NS) solver named *Asphodele* [40–42], developed at the clean combustion laboratory CORIA in Rouen, France. The code allows the simulation of two-phase flows with dispersed particles using Eulerian/Lagrangian method. Several physical models dedicated to collision, combustion and evaporation are developed. The low-Mach number approximation (LMN) is adopted for the solution of the NS equations since the effects of acoustic waves are not considered in this study. The implementation of the submerged body as well as its interaction with the drops follows the work of Briscolini *et al.* [43].

3. Problem setup

The computational setup, shown in Fig. 2, consists of a two-dimensional domain with a length $L_x = 6.318$ *mm* and a width $L_y = 3.159$ *mm*, discretized with a cartesian mesh having $N_x \times N_y = 800 \times 400$ grid points. This discretization allows a good description of the flame properties, since almost twenty points are located within the flame thickness [44]. The time step and mesh size are chosen to meet the CFL conditions.

The domain entrance is on the left and its exit on the right. The borders along the vertical y axis are periodic. The heated cylinder has a diameter of $d_c = 0.632$ *mm* which can be assumed as a hot wire in the experiments. The cylinder temperature is raised up to 1850 K.

The injected fluid is air at ambient pressure with a velocity of $u_0 = 5$ m/s. A mono-dispersed spray is also injected at the same speed with 1 droplet per mesh cell. More physical properties of the gas and dispersed phase can be found in Table 1. The characteristic evaporation time is set to $\tau_v = 63$ μs for n-heptane droplets of diameter $d_p = 1.8$ μm. The flow Reynolds number, based on the cylinder diameter, the flow velocity and the injection velocity, is $Re = 200$.

Physically, for the droplets of the same composition, the characteristic times τ_p and τ_v are related to each other. A change in a droplet diameter induces simultaneous variation of these two parameters, and it is difficult to draw general conclusions regarding the influence of each parameter. In this study, we propose to vary only τ_p by changing particle diameters, such as to examine the influence of solely Stokes number St of droplets on the flame structure. In order to control the variables, the characteristic evaporation time scale τ_v is artificially set to be constant. However, the diameter of the droplets still has an important impacts on the evaporation process. The initial mixture is at stoichiometric conditions and the injected fuel is exclusively liquid.

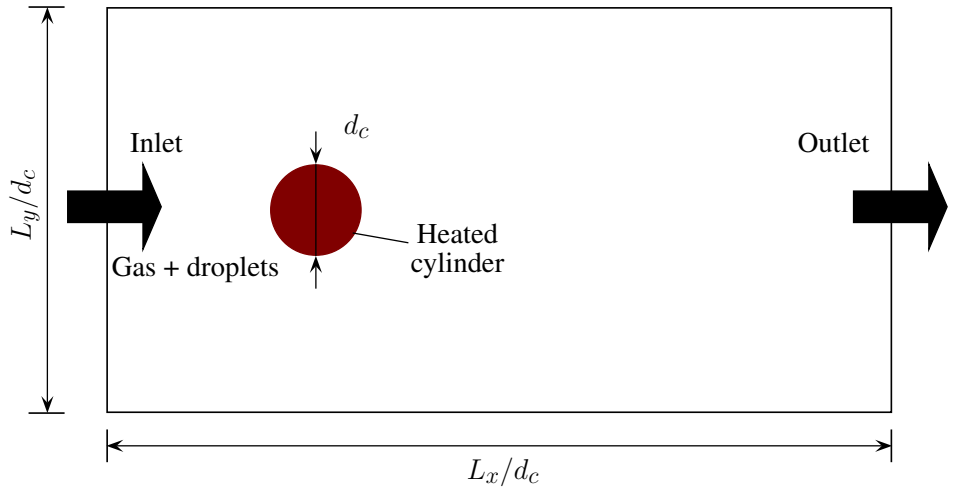

Figure 2: Sketch of the computational domain, with $L_x/d_c = 10$, $L_y/d_c = 5$ and $d_c = 0.632$ *mm* is the diameter of the cylinder.

Three sets of simulations are carried out, by varying the Stokes number of the droplets. The simulations parameters are listed in Table 2. The characteristic time of the flow τ_e is:

$$\tau_e = \frac{d_c}{u_0}\,, \tag{11}$$

and the Stokes number St is defined as:

$$St = \frac{\tau_p}{\tau_e}\,, \tag{12}$$

The flame characteristic time, τ_{fl}, is given by:

$$\tau_{fl} = \frac{\delta_{fl}}{S_L}\,. \tag{13}$$

where δ_{fl} is the flame thickness and S_L the laminar flame velocity.

The Weber number is defined as $We = \rho_g v^2 l/\sigma$, with ρ_g being the air mass density, σ the surface tension, v the relative velocity between the two phases and l being a length scale, usually taken as the droplet diameter. For $We > 80$, the drops disintegrate during the droplet-wall collision process [45, 46]. For droplets in airflow, the critical Weber number for fragmentation is $We_c \approx 12$. In the gas flow of $u_0 = 5\ m/s$, the critical Weber number can be obtained for drops with diameters larger than 100 μm. The range of droplet Weber number chosen here is much lower $3\times10^{-3} < We < 1.8\times10^{-2}$ compared to the critical Weber number, so the drops can be considered as perfectly elastic when rebounding on the cylinder [5, 6].

We also assume that the catalysis effect on the heated cylinder surface is negligible, given the simplicity of the used chemistry model that allows to neglect the effects of the heated body on the radicals.

Simulations	τ_p [μs]	τ_p/τ_{fl}	St [$-$]	Evaporation	Chemistry
$C_{\mathscr{D}_1}$	6.318	1.10^{-3}	0.05	off	off
$C_{\mathscr{D}_2}$	63.18	1.10^{-2}	0.50	off	off
$C_{\mathscr{D}_3}$	315.9	5.10^{-2}	2.50	off	off
$C_{\mathscr{E}_1}$	6.318	1.10^{-3}	0.05	on	off
$C_{\mathscr{E}_2}$	63.18	1.10^{-2}	0.50	on	off
$C_{\mathscr{E}_3}$	315.9	5.10^{-2}	2.50	on	off
$C_{\mathscr{C}_1}$	6.318	1.10^{-3}	0.05	on	on
$C_{\mathscr{C}_2}$	63.18	1.10^{-2}	0.50	on	on
$C_{\mathscr{C}_3}$	315.9	5.10^{-2}	2.50	on	on

Table 2: Summary of the simulated test cases.

4. Study of droplet segregation

The droplet number density is an important quantity from which one can directly deduce the local amount of available gas fuel. In droplet-laden flows, the segregation of droplets is much discussed in terms of Stokes number in the literature [47]. Downstream of the cylinder, the fluid is mainly unsteady in the cylinder wake region and the Stokes number has a direct impact on the droplet segregation. However, in the upstream region, the collisions between the droplets and the submerged body have a dominant effect on the droplet evaporation as well as on the fluid mixture properties in the vicinity of the cylinder. For simplicity, a one-way formalism is used in this study to analyze the phenomenon of the droplet segregation depending on St. This means that only the effect of the gas on the droplets is considered and the gas is assumed not to be affected by the dynamics of the dispersed droplets.

4.1. Effects of St on droplet/body collisions

Three sets of simulations ($C_{\mathscr{D}_1}$, $C_{\mathscr{D}_2}$, $C_{\mathscr{D}_3}$) are first investigated. In these cases, no flame is considered in the two-phase flow and the droplets are taken as rigid particles without evaporation. Figure 3a shows the streamline contours downstream of the cylinder. Basically, the lighter droplets follow the streamline as a result of weak inertia. One can assume that for small droplets with low Stokes numbers and low volume fractions, no collisions occur [48]. The slip velocity $\vec{u}_g - \vec{v}_d$ of the lightest drops remains small at any given point in the field as shown in Fig. 4a. In addition, since the gas in contact with the cylinder is at rest, the droplets cannot touch the cylinder. This effect has also been considered by Pawlowski in 1984 [14].

Collisions between the droplets and the submerged body are more frequent and significant as τ_p increases. The large droplets coming from the front of the cylinder are more likely to collide with the body, because they cannot be deviated by the flow. Drop deviation is more important as one moves away from the center of the domain, where the fluid bypasses the cylinder. The more ballistic the droplets are, the less they will be sensitive to the flow deviation. Thus the large droplets are able to collide with the cylinder even away from the centerline. This phenomenon is schematically represented in Fig. 5, showing the trajectories of drops for both moderate and high Stokes numbers.

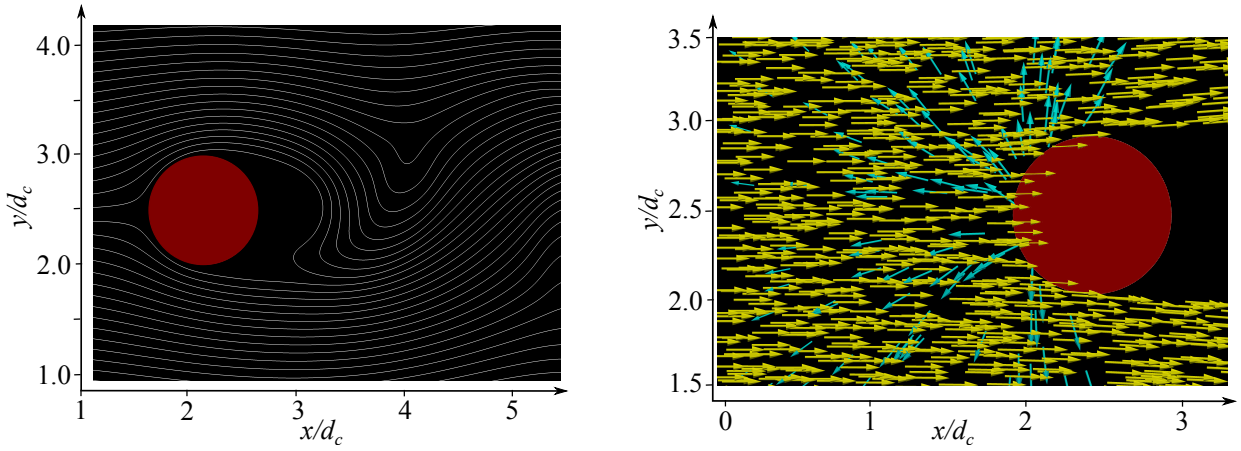

Figure 3: Streamline contours of fluid flow and velocity vectors of drops in the vicinity of the cylinder; (a) gas streamline (b) velocity vectors of the drops with rebound on the cylinder ($St = 2.5$), impinging droplets (→) and bounced droplets (←).

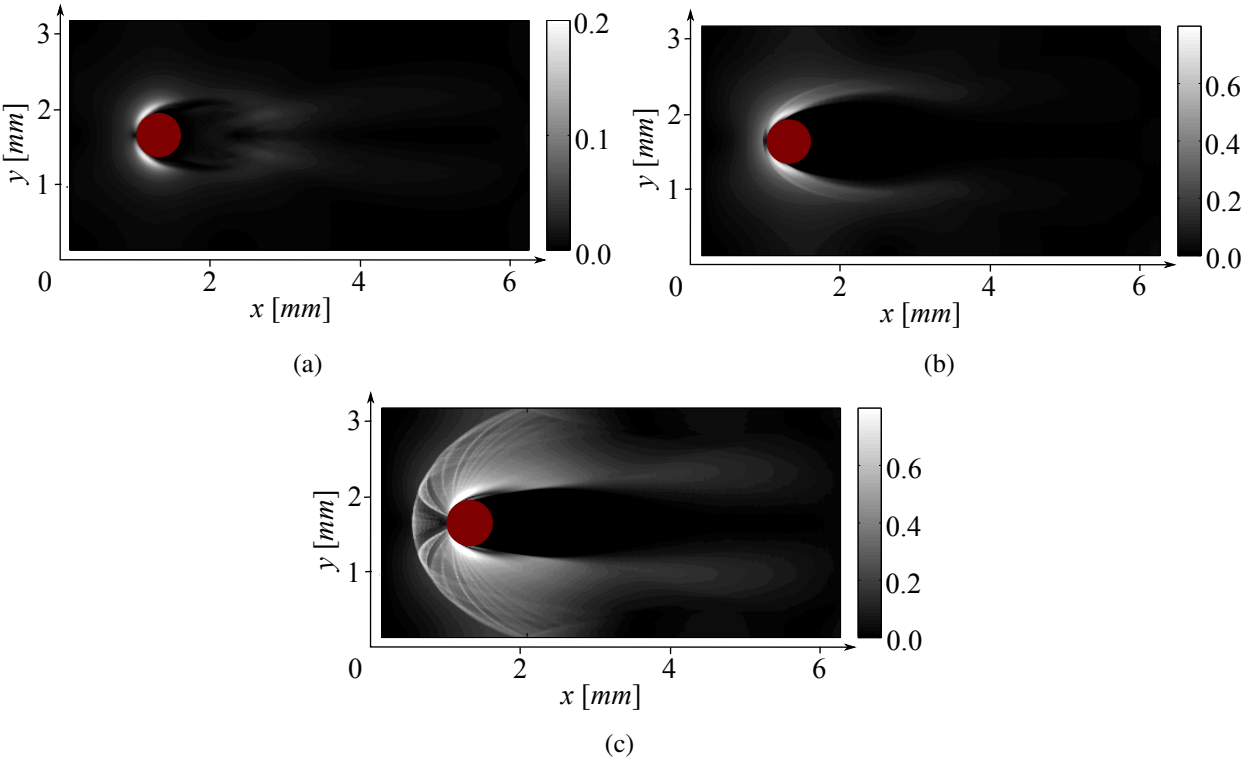

Figure 4: Droplets averaged slip velocity $[m/s]$ for different Stokes numbers St. (a) $C_{\mathscr{D}_1}$: $St = 0.05$, (b) $C_{\mathscr{D}_2}$: $St = 0.5$, (c) $C_{\mathscr{D}_3}$: $St = 2.5$.

Upstream of the cylinder, the droplets can evaporate when approaching the cylinder due to the heat released by the cylinder that significantly increases the temperature of the gas. Consequently,

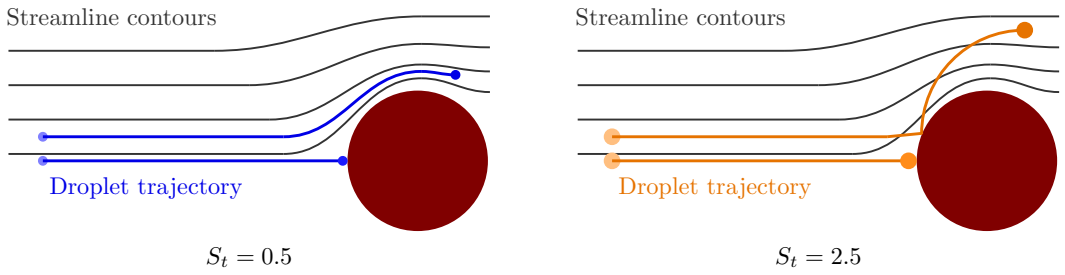

(a) (b)

Figure 5: Schematic representation of two drops trajectories with different Stokes numbers (a) $St = 0.5$, (b) $St = 2.5$.

the evaporation is important in the upstream region near the cylinder. Normally, the droplets come closer to the heated surface when they are heavier.

The large droplets can collide with the cylinder, rebound back towards the injection area and then collide a second time. This implies an even stronger evaporation. The drop density in the upstream region will therefore be more important as St increases due to the collisions with the cylinder.

4.2. Effects of St on the droplets density upstream of the interaction

Figures 6a, 6b and 6c show that the upstream droplet density of the cylinder increases for higher Stokes number simulations. A dense layer of drops appears when the collisions become effective. This effect is visible in Fig. 6b which represents the average density of droplet. The most ballistic drops (case $C_{\mathscr{D}_3}$) collide so violently with the cylinder so that they are ejected far away from the cylinder boundary layer. The droplet front intersection in the downstream region which is visible in Fig. 6b disappears, as shown in Fig. 6c.

It is possible to determine approximately the distance of the upstream droplet front to the cylinder considering a constant injection gas velocity ($u_g = u_0$). Assuming that the momentum loss during the collision is negligible, one can express analytically the droplet velocity as well as the position upstream of the cylinder after rebound. Taking the origin of time at the moment when the drop reaches the submerged body, the rebound droplet velocity can be expressed as $u_d(t=0) = -u_0$. The basic configuration is represented in Fig. 7. The relaxation of the droplet velocity is given by $u_d(t) = u_0 - 2\,u_0\,e^{-t/\tau_p}$. After integration one can find the position of the droplet as $x_d(t) = x_0 + u_0\left(t + 2\,\tau_p\left(e^{-t/\tau_p} - 1\right)\right)$, where x_0 is the initial position of the drop, and x_d its current position.

The time when the droplet velocity relaxes to zero is $t_0 = \tau_p\, ln(2)$. We can therefore determine the position of the droplet cloud front:

$$x_{min} = x(t_0 = \tau_p ln(2)) = x_0 + \tau_p u_0\,(ln(2) - 1)\ , \tag{14}$$

The analytical solution given by Eq. (14) is plotted in Fig. 8, with white circles. One can see that the distance of the upstream droplet front is linearly dependent on the Stokes number, under the assumption of constant entrance gas velocity.

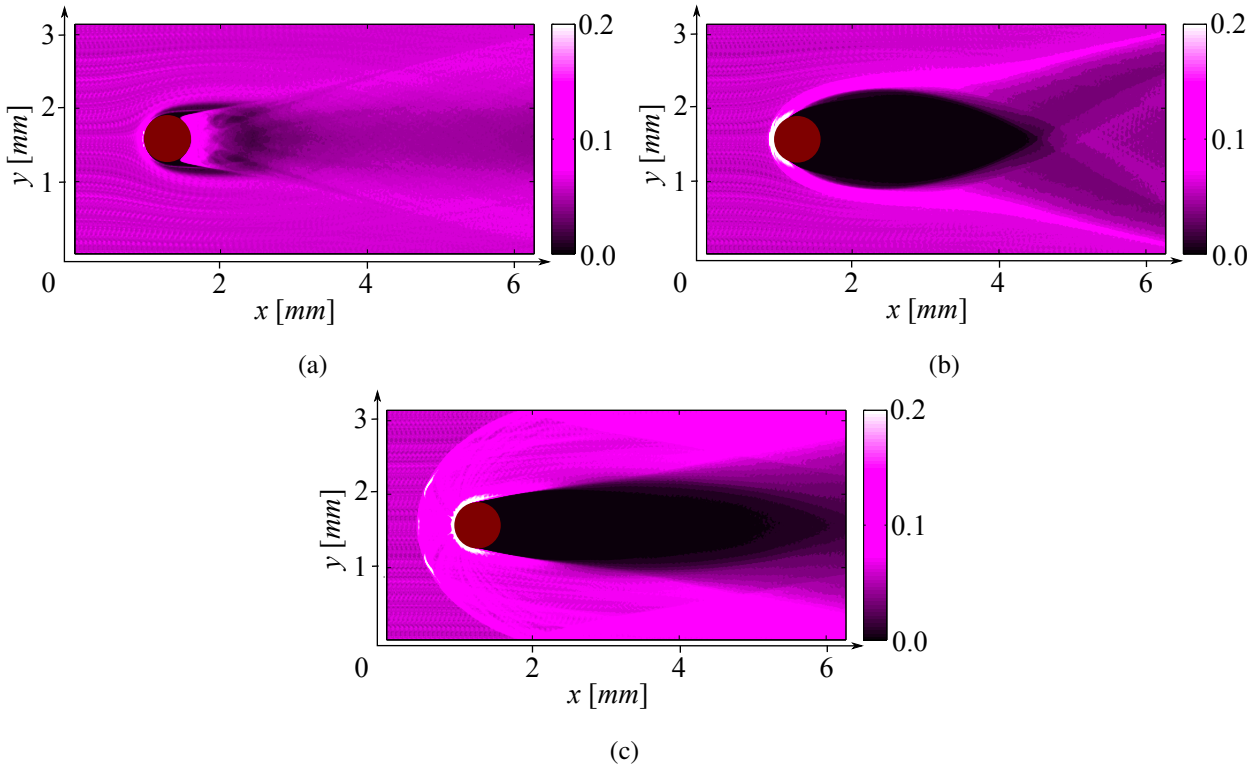

Figure 6: Averaged mass fraction of liquid fuel for different Stokes numbers St, (a) $C_{\mathscr{D}_1}$: $St = 0.05$, (b) $C_{\mathscr{D}_2}$: $St = 0.5$, (c) $C_{\mathscr{D}_3}$: $St = 2.5$.

In order to clarify the effects of the Stokes number on the collision of the upstream droplets, the average values of the droplet density along $x-$axis are plotted in Fig. 8 versus St. We can clearly see that the distance from the droplet cloud front after rebounding is linearly dependent on the Stokes number, which agrees with the analytical solution provided by Eq. (14).

In addition, high values of Stokes number tend to significantly increase the drop density downstream of the cylinder. The mass flow of the liquid fuel that passes through a given cross section S is $Q_v = \iint_S \rho_V \overrightarrow{\bar{u}(S)}.\overrightarrow{dS}$, where ρ_V is the density of the liquid fuel and $\bar{u}$ is the average speed of the drops at a given location as shown in Fig. 4. Since the large droplets are not much evaporated in these cases, the mass flow Q_v of the liquid fuel can be taken as constant over each section of the domain in a stationary regime. Then, a decrease in the average droplet velocity $\bar{u}$ implies an increase in the droplet volume fraction. After rebounding on the cylinder, the large drops are assigned a negative velocity. If τ_p is very large, the time needed for the droplets to catch up the gas velocity cannot be negligible. Thus, upstream the cylinder, the area where the droplets exhibit a low speed presents a high droplet density as shown in Fig. 8.

4.3. Effects of St on the density of drops in the recirculation zone

As shown in Fig. 6a, a recirculation zone is formed downstream of the cylinder. The trajectory of the small drops is close to the streamline and trapped downstream in the reversed flow. Several studies have been carried out to investigate the impact of the Stokes number on the segregation

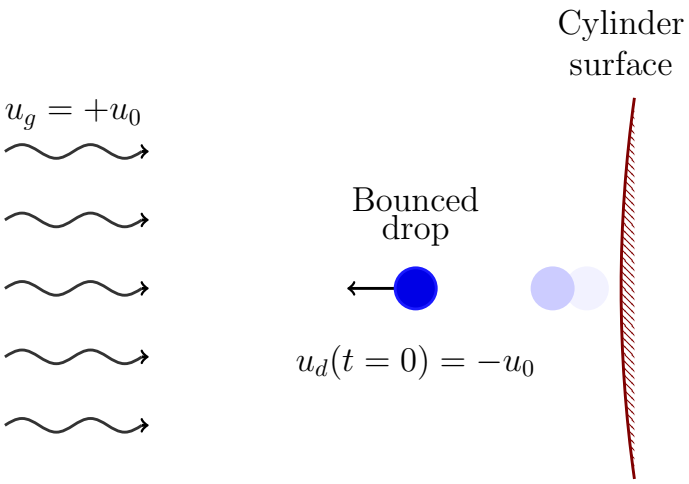

Figure 7: Assumptions made for determining the maximum rebound distance of the drops off the cylinder.

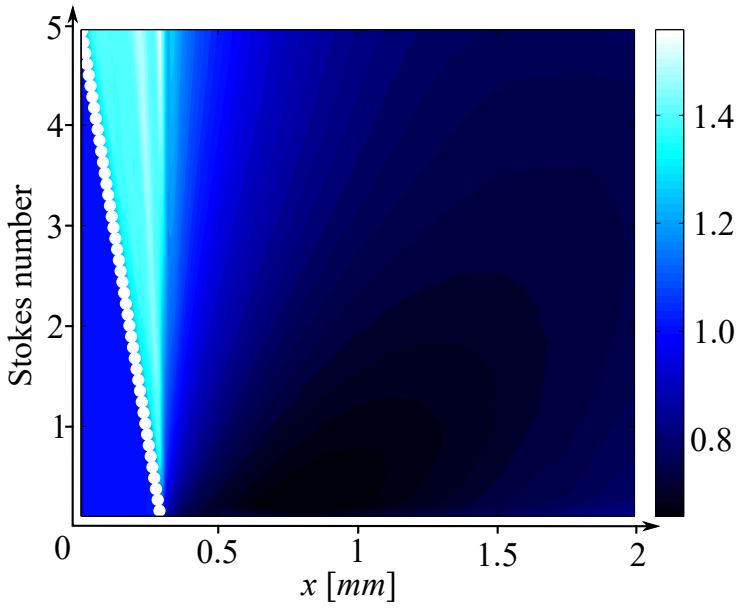

Figure 8: Averaged density of liquid fuel as a function of the Stokes number. White dotted line shows the analytical distance from the front of drops to the cylinder.

of drops in turbulent wake flows [49]. One can deduce that the least ballistic drops will be easily carried in the wake of the cylinder by the von-Kárman instabilities.

5. Characteristics of the gas mixture and the reacting zone

The segregation of the droplets described above illustrates the effects of the Stokes number on the gas mixture during the evaporation of the droplets. This helps us to understand the structure of a flame.

In the simulation $C_{\mathscr{E}_1}$, in which very small droplets are considered, few collisions exist between the drops and the cylinder. The droplets follow the streamline as shown in Fig. 3a. As the droplets never get close to the cylinder surface, their evaporation is relatively weak in the vicinity of the cylinder, as shown in Fig. 9a. The farther the droplets are from the cylinder, the less they will be exposed to the wall-heat release. Consequently, the small droplets can hardly reach favorable conditions for evaporation in the upstream region. However, their small inertial forces make them easier to be dragged into the re-circulation region, which is also affected by the cylinder heating. The lightest drops will therefore be partially evaporated upstream of the cylinder but much more downstream in the recirculation region.

For a significant increase in the ballistics of the spray, such as in case $C_{\mathscr{E}_3}$, the droplets can easily collide with the cylinder. In this limiting case, the droplet front appears as shown in Fig. 9b. The distance from the droplet front, where a relatively high droplet concentration is noticed, to the cylinder surface increases linearly with the relaxation time τ_p of the droplets. In this region, a number of rebounded, partially evaporated droplets, can re-collide with the cylinder. At each rebound, a quantity of gaseous fuel is deposited in the vicinity of the cylinder.

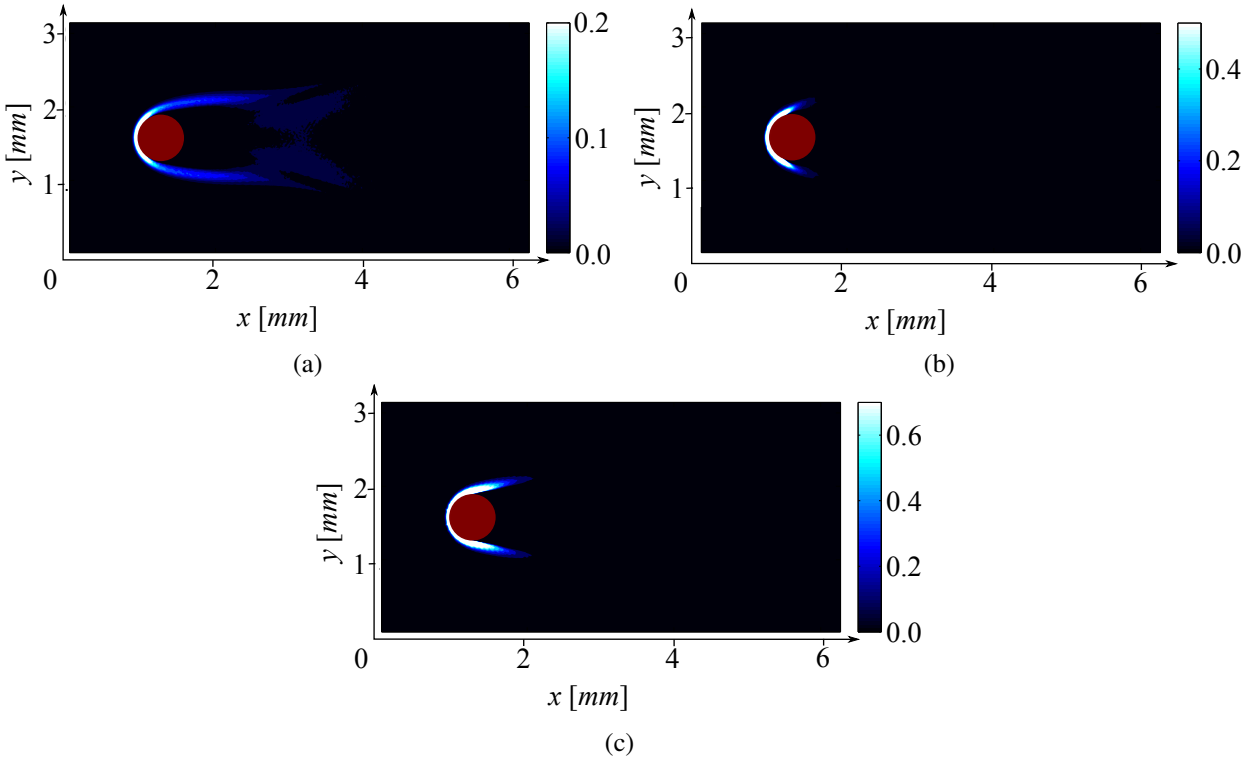

Figure 9: Averaged evaporation rate of the drops for different Stokes numbers, (a) $C_{\mathscr{E}_1}$: $St = 0.05$, (b) $C_{\mathscr{E}_2}$: $St = 0.5$, (c) $C_{\mathscr{E}_3}$: $St = 2.5$.

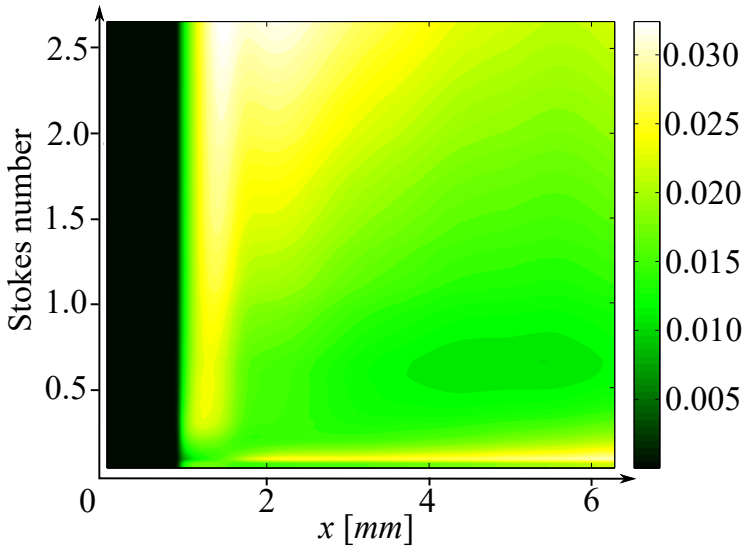

Figure 10: Averaged mass fraction of gaseous fuel as a function of the Stokes number.

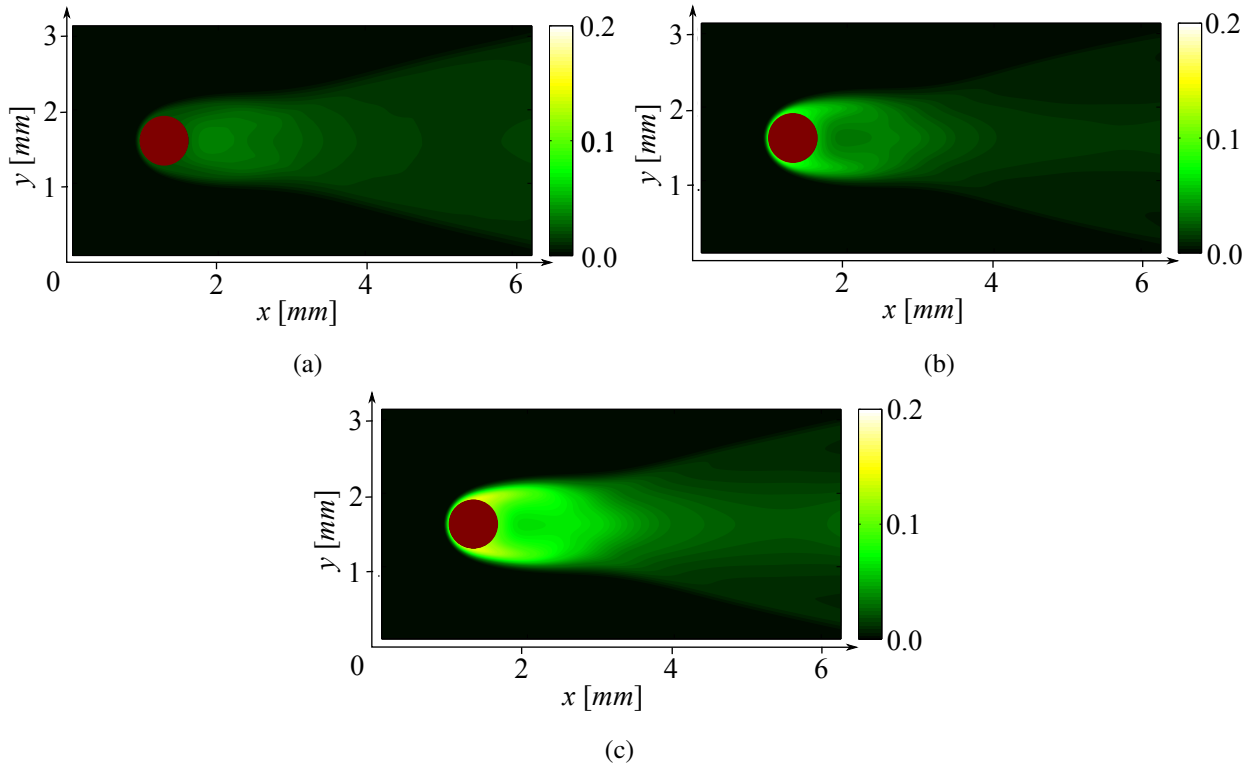

Figure 11: Averaged mass fraction of gaseous fuel for different Stokes number, (a) $C_{\mathscr{E}_1}$: $St = 0.05$, (b) $C_{\mathscr{E}_2}$: $St = 0.5$, (c) $C_{\mathscr{E}_3}$: $St = 2.5$.

The averaged fuel mass fraction along the x-axis as a function of the Stokes number is plotted in Fig. 10. One can notice an increase of the gaseous fuel density around the cylinder when the

Stokes number increases. For droplets of very high Stokes number, as a result of rebounding on the cylinder, the drop density upstream of the cylinder is high. A higher evaporation rate brings more fuel in the gas phase. Very small droplets can follow the gas and can be dragged in the von-Karman valley downstream. They spread into the hot region thus can be much evaporated in the wake region. For intermediate-size droplets, the particles are too heavy to be dragged into the hot zone, but too light to rebound significantly to the upstream of the cylinder, thus they evaporate much less than the others. This explains the formation of a darker region at the right part of Fig. 10.

In order to elucidate the effects of the Stokes number on the combustion, it is necessary to understand its effects on the quantity of the liquid fuel as well as the mixture composition of the gaseous fuel.

As discussed before, the amount of fuel around the cylinder increases with St. The flammable area will therefore be related to the Stokes number. For small droplets, the evaporation is neglected in the vicinity of the cylinder. For droplets with a very high Stokes number, such as in case $C_{\mathscr{C}_3}$, the amount of gaseous fuel around the cylinder is too high to be ignited. This explains why one can notice a detached flame structure in the average reaction rate, shown in Fig. 12c.

In case $C_{\mathscr{C}_2}$, the amount of fuel around the cylinder is lower (see Fig. 11b), which leads to a combustion in the region closer to the cylinder with an attached flame structure.

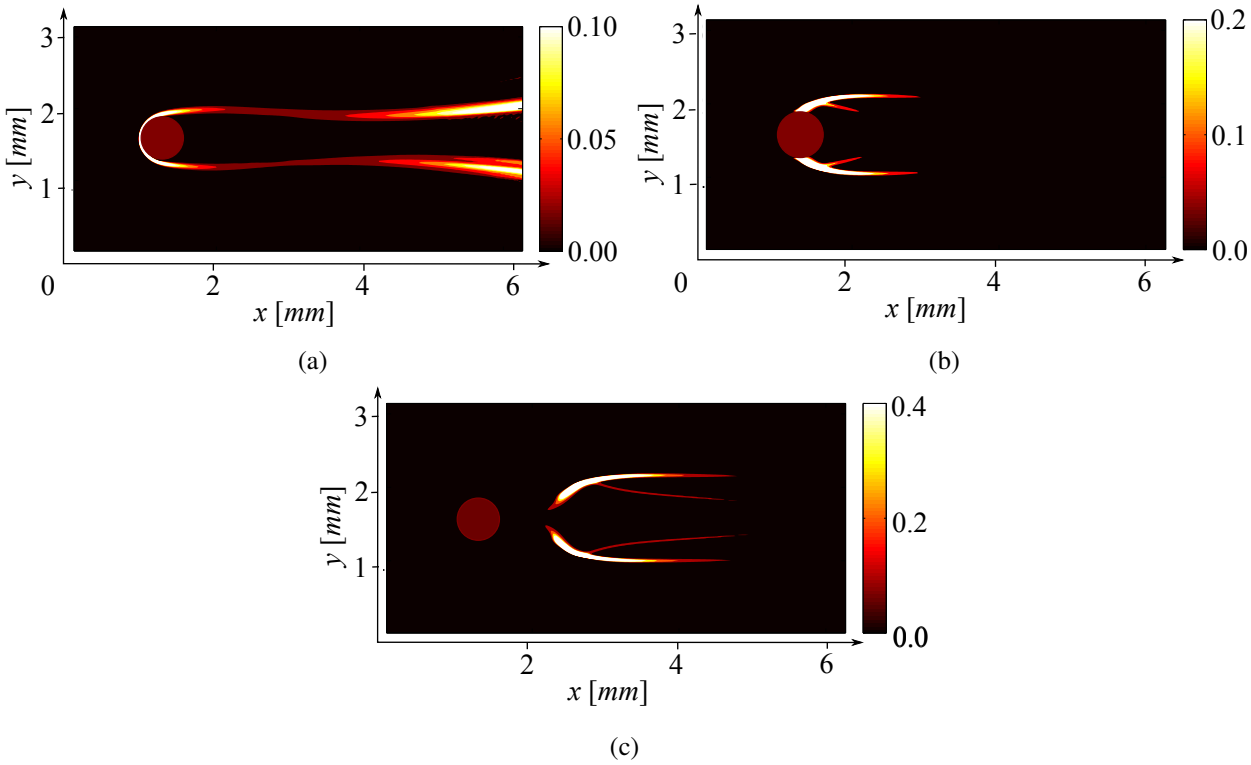

Figure 12: Averaged reaction rate for different Stokes numbers, (a) $C_{\mathscr{C}_1}$: $St = 0.05$, (b) $C_{\mathscr{C}_2}$: $St = 0.5$, (c) $C_{\mathscr{C}_3}$: $St = 2.5$.

In case $C_{\mathscr{C}_1}$, for a spray of small Stokes number, the fuel quantity is sufficient to meet the flammability in the vicinity of the cylinder. In the wake of the cylinder, the drops continue to

evaporate as depicted in Figs. 9a, 10 and 11a. Comparison of cases $C_{\mathscr{C}_1}$ and $C_{\mathscr{C}_2}$ shows that an increase in the Stokes number yields to a fuel increase in the vicinity of the cylinder. However, in case $C_{\mathscr{C}_2}$, the larger droplets are more difficult to be dragged to the wake region. The flame attached to the cylinder is unable to propagate downstream, since the liquid droplets are too far from the heated wake region. In this case, the flame gets trapped in the wake close to the cylinder, as shown in Figs. 12b.

For the most ballistic droplets, the simulations show that a significant quantity of gaseous fuel exist around the cylinder. This region contains a rich mixture that is difficult to ignite, which leads to the detachment of the flame from the cylinder. The region between the cylinder and the flame allows good mixing of fresh gas and the evaporated fuel. As depicted in Fig. 12c, a premixed flame is contained in the rich mixture of the wake region. Then, the remaining excess fuel passes through the premixed flame towards the less mixed wake of the cylinder. A diffusion flame appears afterwards in the wake region as seen in Fig. 12c.

In order to effectively reduce the simulation time, the one-step chemical reaction is used for the description of the combustion process. With this simplified combustion model, some physical phenomena may not be properly described, such as the autoignition delay, the emission of pollutants, etc. Another limitation of the combustion model is that some 3D phenomena may be missed such as the crossing of the flame by the droplets (especially on the surface of the cylinder). Special caution should be taken to account when interpreting the simulation results using such modeling approaches. However, a simple chemical mechanism can be sufficient for the understanding of the dynamics and interactions between the evaporating droplets and the heated cylinder. The objective here is to analyze the main interaction mechanisms between the flame and droplets.

A sketch summarizing the most important physical phenomena encountered in this sophisticated flow is given in Fig. 13. The modification of the Stokes number directly influences the drag of the drops by the downstream unsteady flow (Karmann vortex street). For higher Stokes numbers, the rebound of droplets on the cylinder leads to two distinguished phenomena. First, an increase of the gaseous fuel around the cylinder is noticed. This quantity is higher as the number of Stokes increases. Especially, when the flammability limit is exceeded, the flame detaches from the cylinder surface towards the wake region. The second is the changement of the liquid fuel density distribution around the cylinder wake. Contrary to the small droplets, which can be dragged into the wake region, the larger ones can form a droplet layer around the cylinder. The combustion flame structure is noticed to be contained inside the droplet layer.

6. Conclusions

Numerical simulations are carried out in order to investigate the the impact of the Stokes number on topology of droplet segregation and the density of the droplets. The study highlights new regions of highest density of liquid fuel around the heated cylinder, due to the segregation process in the wake flow past the cylinder. The results show that once the droplets evaporate they introduce gaseous fuel into the concerned area. The topology of the mixture is directly modified by the local density of the drops and therefore by τ_p. The change of Stokes number induces modifications in the mixing properties of the gas fuel. Furthermore, a combustion study is carried out, showing the impact of ballistic drops on the topology of the flame, as well as on its propagation. The detachment of the flame from cylinder is proved to be closely related to the Stokes number. Comparing the wake and the other regions, the unsteady flow can directly enhance the mixing of the fuel and

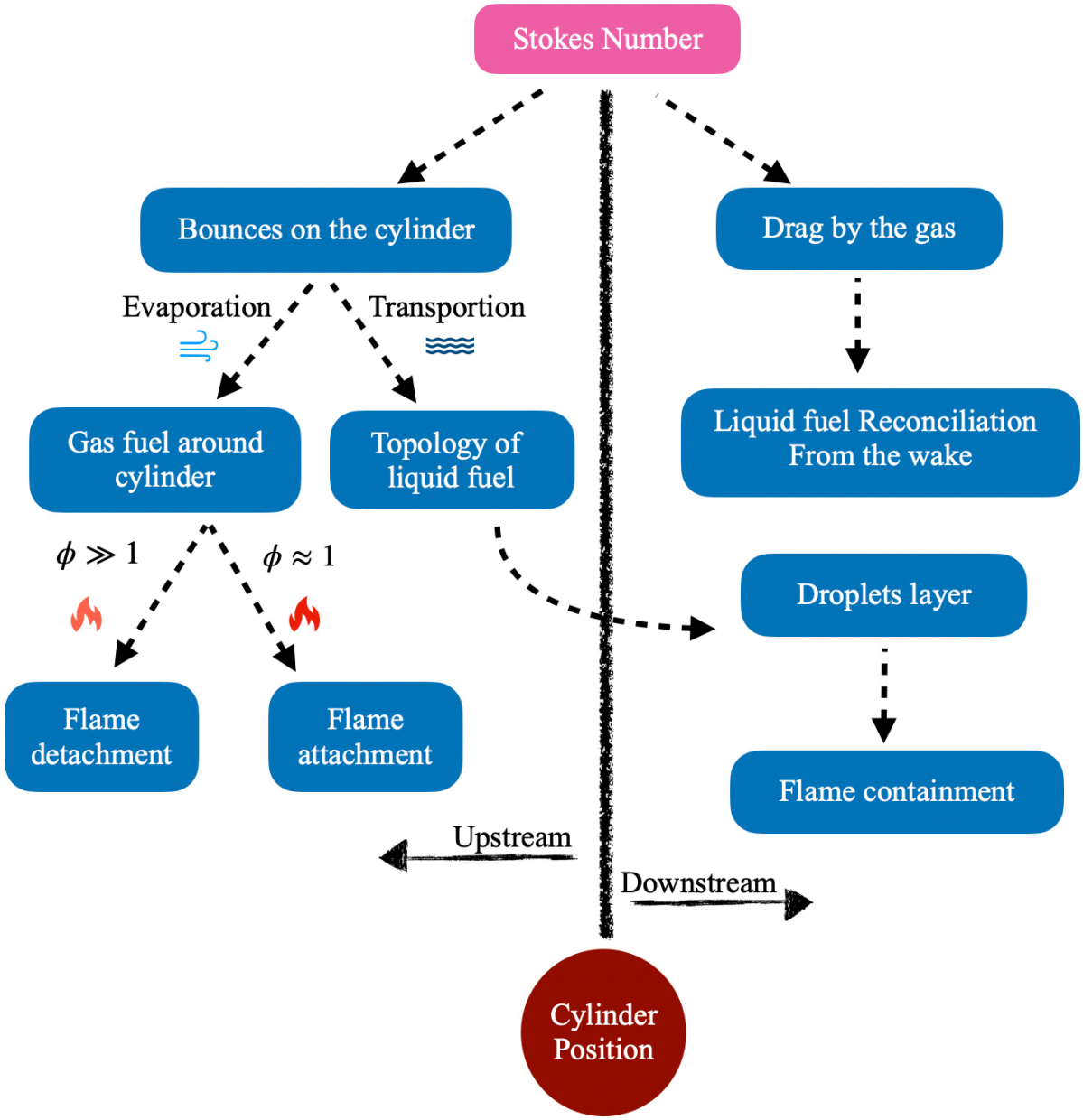

Figure 13: Relationship between different phenomena in the context of the current study, ϕ being the equivalent ratio of the fuel.

air. For a turbulent two-phase incident flow, the premixed combustion region could be larger than the laminar regime. And a higher burning rate could be expected for the premixed flames in the wake region. The diffusion flame could have less regular structures. Other parameters deserve to be studied, such as the richness of the liquid fuel, as well as the characteristic time of the droplet evaporation. Also, a full study could be considered as part of the analysis of flame stability in experimental or industrial devices. Further analysis using a detailed chemical mechanism can be carried out for the quantitative validation of the phenomena observed.

Data Availability

The data that support the findings of this study are available from the corresponding author upon reasonable request.

References

[1] H.D. Landahl and R.G. Herrmann. Sampling of liquid aerosols by wires, cylinders, and slides, and the efficiency of impaction of the droplets. *J. Colloid Sci.*, 4(2):103–136, 1949.

[2] S. Rehman. Hot surface ignition and combustion characteristics of sprays in constant volume combustion chamber using various sensors. *Cogent Eng.*, 5(1), 2018.

[3] P. Xavier, A. Ghani, D. Mejia, M. Miguel-Brebion, M. Bauerheim, L. Selle, and T. Poinsot. Experimental and numerical investigation of flames stabilised behind rotating cylinders: interaction of flames with a moving wall. *J. Fluid Mech.*, 813:127–151, 2017.

[4] S. Lee, J. Park, P. Lee, and M. Kim. Heat transfer characteristics during mist cooling on a heated cylinder. *Heat Transfer Eng.*, 26(8):24–31, 2005.

[5] A. Karl and A. Frohn. Experimental investigation of interaction processes between droplets and hot walls. *Phys. Fluids*, 12(4):785–796, 2000.

[6] S.-L. Chiu and T.-H. Lin. Experiment on the dynamics of a compound drop impinging on a hot surface. *Phys. Fluids*, 17(12):122103, 2005.

[7] Y. Liao, P. D. Eggenschwiler, R. Furrer, M. Wang, and K. Boulouchos. Heat transfer characteristics of urea-water spray impingement on hot surfaces. *Int. J. Heat Mass Transf.*, 117:447 – 457, 2018.

[8] Lily, B. Munshi, K. Barik, and S.S. Mohapatra. The role of surface tension and viscosity of the coolant on spray cooling performance of red-hot inclined steel plate. *Int. J. Heat Mass Transf.*, 130:496 – 513, 2019.

[9] V.S. Papapostolou, C. Turquand d'Auzay, G. Ozel Erol, and N. Chakraborty. Edge flame propagation statistics in igniting monodisperse droplet-laden mixtures. *Phys. Fluids*, 31(10):105108, 2019.

[10] J.W. Buckel and S. Chandra. Hot wire ignition of hydrogen-oxygen mixtures. *Int. J. Hydrog. Energy*, 21(1):39–44, 1996.

[11] P. Stathopoulos, K. Ninck, and Ph. Rudolf von Rohr. Hot-wire ignition of ethanol–oxygen hydrothermal flames. *Combust. Flame*, 160(11):2386 – 2395, 2013.

[12] C. Letty. *Étude d'une flamme en V diphasique. Approches expérimentale et numérique.* PhD thesis, INSA Rouen, France, 2008.

[13] D.O. Glushkov, G.V. Kuznetsov, P.A. Strizhak, and R.I. Taburchinov. Numerical simulation of gel fuel gas-phase ignition by a local source of limited heat content. *Acta Astronaut.*, 163:44 – 53, 2019.

[14] M. Pawlowski and B. Simon. Calculating liquid droplets setting on a cylinder in gas-liquid spray flow. *Int. J. Heat Fluid Fl.*, 5(3):179–184, 1984.

[15] I. Allais, G. Alvarez, and D. Flick. Analyse du transfert thermique entre un cylindre et un écoulement d'air faiblement chargé en gouttelettes d'eau. *Rev. Gen. Therm.*, 36(4):276–288, 1997.

[16] C. Basilico. *Étude du transfert convectif entre un cylindre chauffé et un écoulement d'air chargé de gouttelettes d'eau.* PhD thesis, Institut National Polytechnique de Lorraine, France, 1979.

[17] M.S. Bhatti and C.W. Savery. Augmentation of heat transfer in a laminar external boundary layer by the vaporization of suspended droplets. *J. Heat Transfer*, 97(2):179–184, 05 1975.

[18] T. Aihara. Augmentation of convective heat transfer by gas-liquid mist. *ASME IHTC Jerusalem KN-29*, pages 445–461, 1990.

[19] F.M. Tenzer, I.V. Roisman, and C. Tropea. Fast transient spray cooling of a hot thick target. *J. Fluid Mech.*, 881:84–103, 2019.

[20] J.R. Dawson, R.L. Gordon, J. Kariuki, E. Mastorakos, A.R. Masri, and M. Juddoo. Visualization of blow-off events in bluff-body stabilized turbulent premixed flames. *Proc. Combust. Inst.*, 33(1):1559–1566, 2011.

[21] S. Chaudhuri and B.M. Cetegen. Blowoff characteristics of bluff-body stabilized conical premixed flames with upstream spatial mixture gradients and velocity oscillations. *Combust. Flame*, 153(4):616–633, 2008.

[22] S. Chaudhuri, S. Kostka, M. W. Renfro, and B.M. Cetegen. Blowoff dynamics of bluff body stabilized turbulent premixed flames. *Combust. Flame*, 157(4):790–802, 2010.

[23] L. Yuan. Ignition of hydrolic fluid sprays by open flames and hot surfaces. *J. Loss. Prevent. Proc.*, 19(4):353–361, 2006.

[24] D. Papailou, P. Koutmos, and A. Bakrozis. Simulations of fuel injection and flame stabilization in the wake formation region of a slender cylinder. *Proc. Combust. Inst.*, 28(1):91–99, 2000.

[25] M. Mikami, Y. Maeda, K. Matsui, T. Seo, and L. Yuliati. Combustion of gaseous and liquid fuels in meso-scale tubes with wire mesh. *Proc. Combust. Inst.*, 34(2):3387 – 3394, 2013.

[26] A. Carlos Fernandez-Pello. Micropower generation using combustion: Issues and approaches. *Proc. Combust. Inst.*, 29(1):883 – 899, 2002. Proceedings of the Combustion Institute.

[27] J. Greenberg, I. Silverman, and Y. Tambour. On droplet enhancement of the burning velocity of laminar premixed spray flames. *Combust. Flame*, 113:271–273, 1998.

[28] M. Lawes and A. Saat. Burning rates of turbulent iso-octane aerosol mixtures in spherical flame explosions. *Proc. Combust. Inst.*, 33(2):2047 – 2054, 2011.

[29] G.O. Erol and N. Chakraborty. Inertial effects on globally stoichiometric spherically expanding turbulent flames propagating in droplet-laden mixtures. *Proc. Combust. Inst.*, 2020.

[30] S. Chandrasekhar. Hydrodynamic and hydromagnetic stability. *Oxford University Press.*, pages 11–14, 1961.

[31] D.B. Spalding. *Some Fundamentals of Combustion*. Butterworths, 1955.

[32] G.A.E. Godsave. Studies of the combustion of drops in a fuel spray—the burning of single drops of fuel. *Symposium (International) on Combustion*, 4(1):818 – 830, 1953.

[33] C.K. Law and W.A. Sirignano. Unsteady droplet combustion with droplet heating—ii: Conduction limit. *Combust. Flame*, 28:175 – 186, 1977.

[34] B. Abramzon and W.A. Sirignano. Droplet vaporization model for spray combustion calculations. *Int. J. Heat Mass Transfer.*, 32(9):1605 – 1618, 1989.

[35] W.A. Sirignano. *Fluid Dynamics and Transport of Droplets and Sprays*. Cambridge University Press, 2 edition, 2010.

[36] L. Fréret, O. Thomine, J. Reveillon, S. De Chaisemartin, F. Laurent, and M. Massot. On the role of preferential segregation in flame dynamics in polydisperse evaporating sprays. In *Proceeding of the 2010 Summer Program*, pages 383–392. Center for Turbulence Research, Stanford University, January 2011.

[37] B. Leveugle. *Simulation DNS de l'interaction flamme-paroi dans les moteurs à allumage commandé*. PhD thesis, INSA de Rouen, 2012.

[38] O. Thomine. *Development of multi-scale methods for the numerical simulation of biphasic reactive flows*. PhD thesis, University of Rouen, France, November 2011.

[39] K. Canneviere. *Simulation numérique directe de la combustion turbulente diphasique : application à l'étude de la propagation et de la structure des flammes.* PhD thesis, INSA de Rouen, 2003.

[40] J. Reveillon and F.-X. Demoulin. Effects of the preferential segregation of droplets on evaporation and turbulent mixing. *J. Fluid Mech.*, 583:273–302, 2007.

[41] G. Gai, O. Thomine, A. Hadjadj, and S. Kudriakov. Modeling of particle cloud dispersion in compressible gas flows with shock waves. *Phys. Fluids*, 32(2):023301, 2020.

[42] G. Gai, O. Thomine, S. Kudriakov, and A. Hadjadj. A new formulation of a spray dispersion model for particle/droplet-laden flows subjected to shock waves. *J. Fluid Mech.*, 905:A24, 2020.

[43] M. Briscolini and P. Santangelo. Development of the mask method for incompressible unsteady flows. *J. Comput. Phys.*, 84(1):57–75, 1989.

[44] T. Poinsot and D. Veynante. *Theoretical and Numerical Combustion*. Edwards, 2005.

[45] L.M.J Wachters and N.A.J Westerling. The heat transfer form a hot wall to impinging water drops in the spheroidal state. *Chem. Eng. Sci.*, 21(11):1047–1056, 1966.

[46] J. Dewitte. *Modélisation de l'impact d'un brouillard de gouttes en évaporation et sous pression sur une paroi chauffée.* PhD thesis, École Nationale Supérieure de l'Aéronautique et de l'Espace, Toulouse, France, 2006.

[47] M. Manish and S. Sahu. Analysis of droplet clustering in air-assist sprays using voronoi tessellations. *Phys. Fluids*, 30(12):123305, 2018.

[48] S. Elghobashi. On predicting particle-laden turbulent flows. *Appl. Sci. Res.*, 52(4):309–329, June 1994.

[49] J. Reveillon, C. Pera, M. Massot, and R. Knikker. Eulerian analysis of the dispersion of evaporating polydispersed sprays in a statistically stationary turbulent flow. *J. Turb.*, 5:1–27, 2004.